Jurnal Teknologi

Full paper

Realistic Design of a Floating Breakwater Design with Moonpools

Faisal Mahmuddin*, Rahimuddin

Naval Architecture Department, Engineering Faculty, Hasanuddin University, Makassar Indonesia

*Corresponding author: f.mahmuddin@gmail.com

Article history

Received :20 March 2014
Received in revised form :
2 April 2014
Accepted :25 May 2014

Graphical abstract

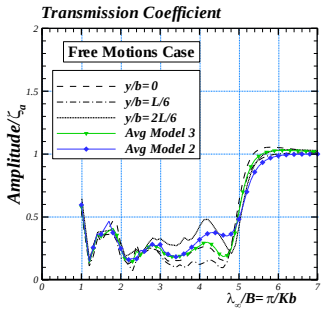

Abstract

In an attempt to obtain a 2D floating breakwater model with high performance in wave reflection, genetic algorithm (GA) was combined with boundary element method (BEM) in the previous study. The performance of the obtained model was verified with numerical relations as well as an experiment in towing tank. Moreover, its performance and characteristics in 3D case were also evaluated in the subsequent study. However, because the 3D model is formed by simply extruding the 2D shape in longitudinal direction, it only produces a model with uniform transversal shape which is considered to be less effective and efficient in terms of technical and economical points of view. Consequently, it is needed to modify the model to obtain a more realistic and efficient design without reducing significantly the high performance obtained previously. In the present study, several modifications of the original 3D model are performed which include placing moonpools inside the body. The performance and characteristics of the modified models in terms of wave elevations on the free surface are evaluated at various wavelengths by using higher order boundary element method (HOBEM). The accuracy of the computed results is confirmed with Haskind-Newman and energy conservation relations. From the modifications and evaluations of the models, it could be realized that the moonpools inside the body could be used to obtain a more realistic model without reducing the optimum performance of the original model shape.

Keywords: Floating breakwater; moonpools; higher order boundary element method (HOBEM); realistic model; transmission coefficient; wave elevation

1.0 INTRODUCTION

It is known that near-shore area has become an increasingly important place for people to conduct activities nowadays. Consequently, it is necessary to protect it from wave attack and other harsh environment conditions. Protectingthe area would enable people to conduct activities in this area conveniently which consequently could increase their productivity as well asthe economic growth around the area.The methods of protection ranging from simple structures such as rubble mound breakwaters[1,2,3] to more complicated structures such as caisson type breakwaters[4,5,6]. However, one of the increasingly popular methods recently is to install a floating-type breakwater[7,8]. This type of floating breakwater has several advantages such as low construction cost, installation flexibility, fresh water preservation, easy repair, etc.

Some of the important matters to consider when choosing a floating breakwater model to be installed are its performance and construction cost. Consequently, less volume models are more preferable since it will be cheaper for construction. Therefore it is important to obtain a model which has less volume without reducing significantly its performance. Moreover, from technical point of view, less material model tends to be lighter. It is known that being lighter is also one of the desirable properties of a floating breakwater.

In a previous study conducted by Mahmuddin and Kashiwagi[9], genetic algorithm (GA) was combined with boundary element method (BEM) to obtain a 2D floating breakwater model shape which has a high performance in wave reflection. The performance of the model in 3D case was also evaluated in a subsequent study[10]. In the present study, the optimized model is modified to obtain a more realistic and efficient floating breakwater model in terms of model volume. It is common that a model with less volume relatively will have less material and weight in constructing the real model.

The original model to be modified was constructed by extruding an optimized 2D shape obtained from a study carried out by Mahmuddin and Kashiwagi[9] into horizontal direction. Consequently, the model has uniform transversal shape which can be considered to be less effective and efficient. Therefore, it is needed to modify this shape to obtain a more realistic and efficient model without reducing significantly the performance obtained previously.

In order to obtain a more realistic model, moonpools will be placed inside the floating breakwater. With the moonpools inside the body, the incident wave would enter the moonpool and make interaction with the water inside the body. Motions and interaction of the incident waves inside the moonpool could be expected to reduce the energy of incident wave which consequently reduce the transmitted wave[11,12]. In order to compare the performance of models withmoonpools, a model with

the same volume reduction in the midst of the model will also be evaluated.

In order to analyze the performance of the modified models, higher order boundary element method (HOBEM) is employed. HOBEM which is based on the potential flow theory divides the body into certain number of panels and represents both quadrilateral panels and unknown velocity potentials with quadratic representation. The hydrodynamic forces, body motions and wave elevations on the free surface around the body can be computed and analyzed with this method.

The accuracy and correctness of the computation results are confirmed with Haskind-Newman and energy conservation relations. In the present study, computations and analysis will be performed only in beam wave case.

■2.0 SOLUTION METHOD

2.1 Mathematical Formulations

The present study is concerned with the development an optimal floating breakwater by optimizing the body shape. Therefore, in order to be able to analyze a model with arbitrary shape, the body shape is assumed to be asymmetric in all directions. The coordinate system adopted is shown in Figure 1, where the body shape isarbitrary and asymmetric with respect to*x*, *y* and *z*-axes.

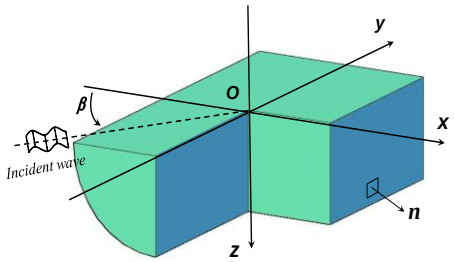

Figure 1 Coordinate system and normal vector definitions

The origin of the coordinate system is placed at the center of the body and on the undisturbed free surface, and the *z*-axis is taken positive vertically downward. The water depth is assumed to be infinite. The regular wave is considered to be incoming with incident angle $\beta$with respect to the negative*x*-axis as shown in Figure 1. Thus β=180 deg. means the wave incoming from the positive *x*-axis(beam wave case) which is considered in the present study.

Under the assumption of incompressible and inviscid flow with irrotational motion, the velocity potential can be introduced, satisfying Laplace's equation as the governing equation. The boundary conditions are linearized and all oscillatory quantities are assumed to be time-harmonic with circular frequencyω. Applying superposition principle, the velocity potential can be expressed as a summation of the incident-wave potential ϕ_0 and the disturbance potential ϕ as follows:

$$\Phi(x,y,z,t) = \mathrm{Re}\left[\left\{\phi_0(x,y,z)+\phi(x,y,z)\right\}e^{i\omega t}\right] \tag{1}$$

where ϕ_0 can be given explicitly as

$$\phi_0(x,y,z) = \frac{g\zeta_a}{i\omega}e^{-Kz-iK(x\cos\beta+y\sin\beta)} \tag{2}$$

With g the acceleration of gravity, ζ_a the amplitude of incident wave, and K the wavenumber given by $K=\omega^2/g$. Furthermore, the disturbance potential ϕ can be decomposed in the following form

$$\phi(x,y,z) = \frac{g\zeta_a}{i\omega}\left[\phi_7(x,y,z) - K\sum_{j=1}^{6}\frac{X_j}{\zeta_a}\phi_j(x,y,z)\right] \tag{3}$$

where ϕ_7 denotes the scattering potential in the diffraction problem, and ϕ_j is the radiation potential in the *j*-th mode of body motion with complex amplitude X_j. In 3D problems, we consider six degrees of freedom in general as shown in (3) which are surge $(j=1)$, sway $(j=2)$, heave $(j=3)$, roll $(j=4)$, pitch $(j=5)$, and yaw $(j=2)$. For the diffraction problem, the sum of $\phi_0+\phi_7$ is denoted as ϕ_D, which is referred to as the diffraction potential in this paper.

The governing equation and boundary conditions to be satisfied can be summarized as follows:

$$[L] \quad \nabla^2\phi_j = 0 \qquad \text{for } z \geq 0 \tag{4}$$

$$[F] \quad \frac{\partial\phi_j}{\partial z} + K\phi_j = 0 \qquad \text{on } z=0 \tag{5}$$

$$[H] \quad \frac{\partial\phi_j}{\partial n} = \begin{cases} n_j & (j=1\sim6) \\ 0 & (j=D) \end{cases} \qquad \text{on } S_H \tag{6}$$

$$[B] \quad \frac{\partial\phi_j}{\partial z} = 0 \qquad \text{as } z\to\infty \tag{7}$$

and also an appropriate radiation condition of outgoing waves must be satisfied for $j=1\sim7$. Here S_H denotes the body wetted surface and n_j the *j*-th component of the normal vector, defined as positive when directing out of the body and into the fluid.

By using Green's theorem, the governing differential equations of the present problem are turned into integral equations on the boundary. That boundary surface can be only the body surface S_H by introducing the free-surface Green function, and the resulting integral equations can be written in the form

$$C(P)\phi_j(P) + \iint_{S_H}\phi_j(Q)\frac{\partial}{\partial n_Q}G(P;Q)\,dS(Q) = \begin{cases} \iint_{S_H} n_j(Q)G(P;Q)\,dS(Q) & j=1\sim6 \\ \phi_0(P) & j=D \end{cases} \tag{8}$$

where $C(P)$ is the solid angle, $P=(x,y,z)$ is the field point, $Q=(x',y',z')$ is the integration point on the body surface. $G(P;Q)$ is the free-surface Green function satisfying the linearized free-surface and radiation conditions, which can be expressed as

$$G(P;Q) = -\frac{1}{4\pi}\left(\frac{1}{r}+\frac{1}{r_1}\right) - \frac{K}{2\pi}G_W\left(R, z+z'\right) \tag{9}$$

Where

$$\left.\begin{matrix} r \\ r_1 \end{matrix}\right\} = \sqrt{(x-x')^2+(y-y')^2+(z\mp z')^2} \equiv \sqrt{R^2+(z\mp z')^2} \quad (10)$$

$$G_W(R,z) = -\frac{2}{\pi}\int_0^\infty \frac{k\sin kz + K\cos kz}{k^2+K^2} K_0(kR)\,dk - i\pi e^{-Kz} H_0^{(2)}(KR) \quad (11)$$

Here $K_0(kR)$ denotes the second kind of modified Bessel function of zero-th order and $H_0^{(2)}(KR)$ the second kind of Hankel function of zero-th order.

2.2 Higher-order Boundary Element Method

In order to attain high accuracy, the integral equation shown above was numerically solved by the Higher-Order Boundary Element Method (HOBEM), described in Kashiwagi[13]. The body surface is discretized into a number of quadrilateral panels. According to the concept of iso-parametric representation, both body surface and unknown velocity potential on each panel are represented with 9-point quadratic shape functions $N_k(\xi,\eta)$ $(k=1\sim 9)$ as follows:

$$\{x,y,z\}^T = \sum_{k=1}^{9} N_k(\xi,\eta)\{x_k,y_k,z_k\}^T \quad (12)$$

$$\phi(x,y,z) = \sum_{k=1}^{9} N_k(\xi,\eta)\phi_k \quad (13)$$

where (x_k,y_k,z_k) are local coordinates at 9-nodal points on a panel under consideration, and likewise ϕ_k denotes the value of the velocity potential (which is to be determined) at 9-nodal points of a panel.

The shape functions in (12) and (13) for a quadrilateral panel can be expressed in the form

$$\left.\begin{aligned} N_k &= \frac{1}{4}\xi(\xi+\xi_k)\eta(\eta+\eta_k) \quad \text{for } k=1\sim 4 \\ N_5 &= \frac{1}{2}\eta(\eta-1)(1-\xi^2), \quad N_6 = \frac{1}{2}\xi(\xi+1)(1-\eta^2) \\ N_7 &= \frac{1}{2}\eta(\eta+1)(1-\xi^2), \quad N_8 = \frac{1}{2}\xi(\xi-1)(1-\eta^2) \\ N_9 &= (1-\xi^2)(1-\eta^2) \end{aligned}\right\} \quad (14)$$

where index k denotes the local node number $(k=1\sim 9)$, as shown in Figure 2.

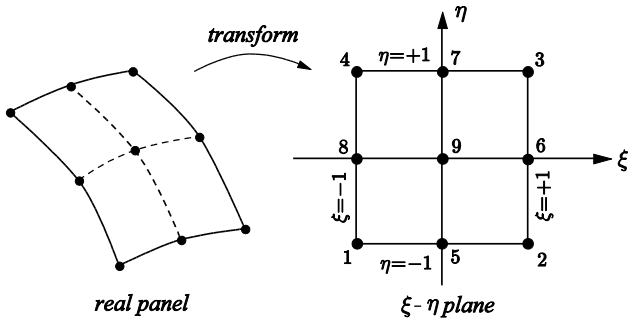

Figure 2 Quadrilateral 9-node Lagrangian element

The normal vector on the body surface (each panel) can be computed with differentiation of the shape function as follows:

$$\boldsymbol{n} = \frac{\boldsymbol{a}\times\boldsymbol{b}}{|\boldsymbol{a}\times\boldsymbol{b}|}, \quad \boldsymbol{a} = \left(\frac{\partial x}{\partial\xi},\frac{\partial y}{\partial\xi},\frac{\partial z}{\partial\xi}\right), \quad \boldsymbol{b} = \left(\frac{\partial x}{\partial\eta},\frac{\partial y}{\partial\eta},\frac{\partial z}{\partial\eta}\right) \quad (15)$$

Through a series of substitution, finally the boundary integral equations can be recast in a series of algebraic equations for the velocity potentials at nodal points consisting of panels. The results can be expressed in the form

$$C_m\phi_m + \sum_{\ell=1}^{NT} D_{m\ell}\phi_\ell = \begin{cases} \sum_{n=1}^{N} S_{mn}^j & j=1\sim 6 \\ & m=1\sim NT \\ \phi_0(P_m) \end{cases} \quad (16)$$

where

$$D_{m\ell} = \iint_{S_n} N_k(\xi,\eta)\frac{\partial G(P_m;Q)}{\partial n_Q}\left|J(\xi,\eta)\right|d\xi d\eta \quad (17)$$

$$S_{mn}^j = \iint_{S_n} n_j(Q)G(P_m;Q)\left|J(\xi,\eta)\right|d\xi d\eta \quad (18)$$

and index n denotes the serial n-th panel, index m the global serial number of nodal points, and $\ell=(n,k)$ is also the serial number of nodal points associated with (to be computed from) the k-th local node within the n-th panel. $|J(\xi,\eta)|$ in(17) and (18) denotes the Jacobian in the variable transformation. NT denotes the total number of nodal points and thus (16) is a linear system of simultaneous equations with dimension of $NT\times NT$ for the unknown velocity potentials at nodal points. The solid angle C_m in (16) is computed numerically by considering the equi-potential condition that a uniform potential applied over a closed domain produces no flux and thus zero normal velocities over the entire boundary.

The free-surface Green function, given by(11), can be computed efficiently by combining several expressions such as the power series, asymptotic expansions, and recursion formulae; its subroutine is available in Kashiwagi *et al.*[14]

2.3 Hydrodynamic Forces

Once the velocity potentials on the body surface are determined, it is straightforward to compute the hydrodynamic forces. The results are written in the form

$$F_{ij} = -\rho \iint_{S_H} \phi_j \, n_i \, dS \equiv A_{ij} - \frac{i}{\omega} B_{ij} \tag{19}$$

$$E_j = \rho g \zeta_a \iint_{S_H} \phi_D \, n_j \, dS \tag{20}$$

where F_{ij} is the radiation force in the *i*-th direction due to the *j*-th mode of motion and its real and imaginary parts are the added mass A_{ij} and damping coefficient B_{ij}. E_j in (20) denotes the wave-exciting force. These quantities are expressed with respect to the origin of the coordinate system shown in Figure 1, and can be combined to obtain corresponding quantities expressed with respect to the center of gravity; which will be used in establishing the motion equations.

The equations of body motion with respect to the center of gravity can be established in a matrix form as follows:

$$\sum_{j=1}^{6} X_j^G \left\{ -K\left(M_{ij}\,\delta_{ij} + F_{ij}^G\right) + C_{ij}^G \right\} = E_i^G \quad \text{for } i = 1 \sim 6 \tag{21}$$

Superscript *G* means quantities with respect to the center of gravity. M_{ij} denotes the generalized mass matrix, δ_{ij} is the Kroenecker's delta, and C_{ij}^G is the restoring-force coefficients due to the static pressure. By solving these coupled motion equations, the complex motion amplitude X_j^G can be determined and then the corresponding complex amplitude with respect to the origin of the coordinate system X_j $(j = 1 \sim 6)$ can be obtained from

$$\left.\begin{aligned} X_j &= X_j^G + \varepsilon_{jkl}\,(x_G)_k\, X_{l+3}^G \\ X_{j+3} &= X_{j+3}^G \end{aligned}\right\} \quad (j = 1 \sim 3) \tag{22}$$

where ε_{jkl} denotes the alternating tensor for the outer product of vectors and $(x_G)_k$ $(k = 1 \sim 3)$ the ordinates of the center of gravity.

The numerical accuracy can be confirmed by checking the Haskind-Newman relation for the wave-exciting force and the energy-conservation relation for the damping coefficient. These relations are expressed as

$$E_j = \rho g \zeta_a H_j(K, \beta) \tag{23}$$

$$B_{ij} = \frac{\rho \omega K}{4\pi} \mathrm{Re} \int_0^{2\pi} H_i(K,\theta) H_j^*(K,\theta)\, d\theta \tag{24}$$

where $H_j(K,\theta)$ denotes the so-called Kochin function in the radiation problem, expressed as

$$H_j(K,\theta) = \iint_{S_H} \left(\frac{\partial \phi_j}{\partial n} - \phi_j \frac{\partial}{\partial n} \right) e^{-Kz - iK(x\cos\theta + y\sin\theta)}\, dS \tag{25}$$

where θ is the angle of radiated wave with respect to minus *x*-axis.

2.4 Wave Elevation on Free Surface

The wave elevation on the free surface in the linear theory can be computed from

$$\frac{\zeta(x,y)}{\zeta_a} = \phi_0(x,y,0) + \phi_7(x,y,0) - K \sum_{j=1}^{6} \frac{X_j}{\zeta_a} \phi_j(x,y,0) \tag{26}$$

where the velocity potentials due to disturbance by a floating body can be computed from

$$\phi_7(P) = -\iint_{S_H} \phi_D(Q) \frac{\partial}{\partial n_Q} G(P;Q)\, dS(Q) \tag{27}$$

$$\phi_j(P) = \iint_{S_H} \left\{ n_j(Q) - \phi_j \frac{\partial}{\partial n_Q} \right\} G(P;Q)\, dS(Q) \tag{28}$$

where $P = (x, y, 0)$ is a point on the free surface.

In HOBEM, these velocity potentials can be computed by using the shape function and the solutions of the velocity potentials at nodal points. The integrals in (27) and (28) can be evaluated by summation over all panels, on which element computations can be done using the same scheme for the coefficients shown in Equations (17) and (18), with *P* placed on the free surface.

In this paper, we are concerned with the transmission and reflection waves by a floating breakwater. The transmission wave is defined by the wave in the lee side, propagating in the same direction as that of the incident wave. On the other hand, the reflection wave must be defined as the wave in the weather side, propagating to the opposite direction. Thus the incident-wave term $\phi_0(x,y,0)$ in Equation (26) is subtracted from Equation (26) in numerical computations for the reflection wave.

4.0 RESULTS AND DISCUSSION

From the previous study conducted by Mahmuddin and Kashiwagi[9], an optimal 2D shape had been obtained. Based on this shape, a 3D model is constructed by extruding it into longitudinal direction. The performance of the 3D model is found to be similar to the 2D one when the body dimension is quite long[10]. The determined 2D shape and its dimension are shown in Figure 3 and Table 1, respectively.

Table 1 also shows geometrical parameters which need to be assumed before computation which are center of gravity (*OG*) and roll gyrational radius (*Kzz*). The same values of these parameters are used in all 3D models computations in this study. The exact value of these parameters can only be known once the real model is constructed.

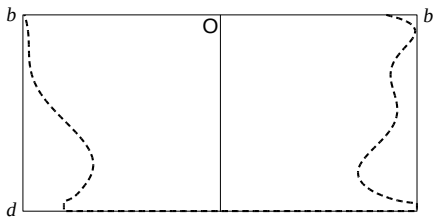

Figure 3 Optimized 2D model shape

Tabel 1 Dimension of 2D model

Notations	Unit
Maximum breadth ($B=2b$)	2.0
Draft (d)	1.0
Center of gravity (OG)	0.82
Roll gyrational radius (Kzz)	0.614

The corresponding 3D model shape and its dimension notations are shown in the Figure 4. As it can be seen from the figure, the transverse sections of the model are uniform. The main goal of the present study is to obtain a realistic model by reducing certain amount of model volume. Reducing the model volume is carried out by removing some portions of the uniform part without significantly reduced the performance of the original model which has been obtained previously.

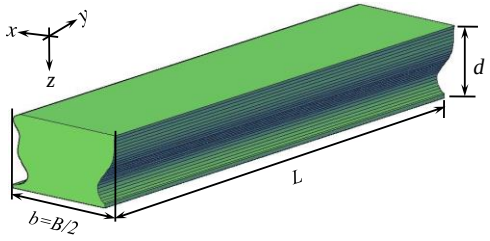

Figure 4 Original 3D model shape

In 2D case, the wave reflection and transmission are easily defined because their magnitudes are same at any position of measurement. However, in 3D computations, the wave elevations will depend on the measurement positions because the wave field around the body will also be in 3D form.

Therefore, in order to compare the wave transmission of 2D and 3D cases, 3 different positions along negative x-axis are defined for waves measurement in 3D case which are at $-x/b =$ 4, 10 and 18 as illustrated in the Figure 5.

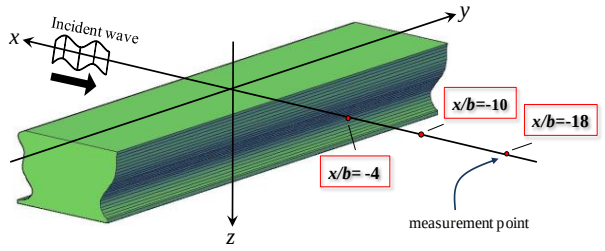

Figure 5 Wave measurement positions in 3D case

The performance of the optimized 2D model compared to original 3D model for body length L/b=40, are found to be similar as shown in the Figure 6. Theoretically, computing much longer body length will make the computed results of 2D and 3D are even more similar.

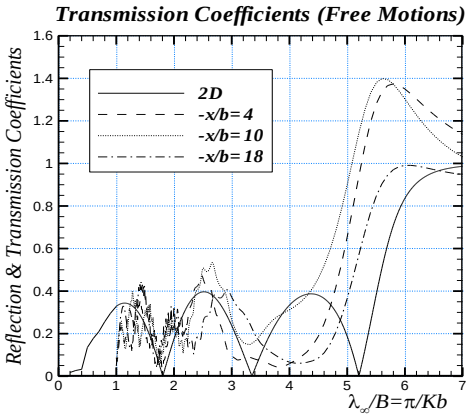

Figure 6 Transmission coefficients of 2D and original 3D models

However, from body shape shown in Figure 4, the original 3D model could be considered to be less efficient in terms of technical and economical points of views due to uniform transversesection as previously explained. Therefore, some modifications of the original 3D model are performed in this study.

In the previous 3D computations, the transmitted waves are only defined by 3 points along x-axis line because the computation results need to be compared with 2D ones. However, because the next modification will be performed in several positions inside the body, the waves will be more complicatedthan in the previous case. Therefore, in order to fairly evaluate the wave transmission, the transmitted wavesare measured in 9 different positions which are 3 positions along y-axis and 3 positions along x-axis as illustrated in Figure 7.

However, only wave transmissions in positive part of x-y plane which will be measured because all models evaluated in this study are symmetric with respect to x-axis so the wave transmission in the negative x-y plane will be same.

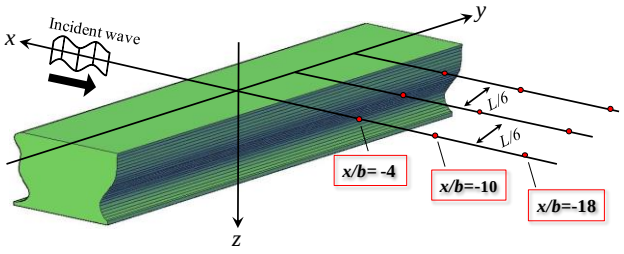

Figure 7 New wave measurement positions

In the analysis, the problem is divided into fixed motions (diffraction) case and free motions case (diffraction + radiation). However, only computation results of free motions case which will be discussed in the present study.

The first modification is performed by reducing the volume of the model in the midst of the model which will be named as Model 1. The shape and dimension notations of Model 1 are shown in the Figure 8.

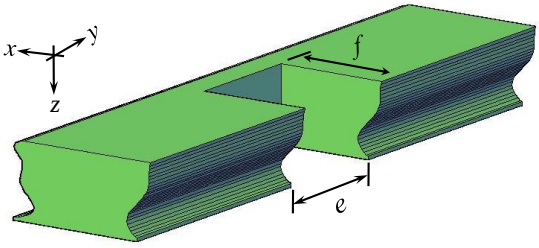

Figure 8 Model 1 shape

The dimensions of reduced part are $e/b=$ 10.667 and $f/b=1.6$. The performance for this model is shown in Figure 9. In this figure, only wave transmission along *y*-axis which will be shown. The computation results in each *y*-axis position are taken as the average of the wave transmission at 3 positions along*x*-axis.

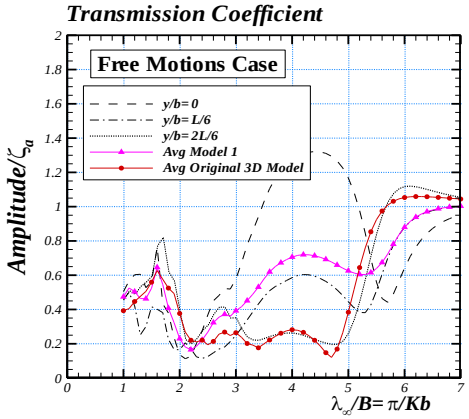

Figure 9 Transmission coefficients of Model 1 and original model

In Figure 9, besides the wave elevations measured in 3 defined positions, the average wave amplitude from these 3 wave amplitudes are also calculated and shown by a delta markedsolid line. Besides that, the average of wave transmission from original model measured in 9 positions (using new measurement definition) is also shown by a rectanglemarkedsolid line.

By comparing the transmitted waves of the original model and Model 1, it is obvious that the performance of the Model 1 is still poor especially in the wavelength λ_∞/B=2.2~5.2. The performance reduction can be attributed to the shape change of the original model. The reason can be justified by observing high transmission coefficient in the measurement position y/b=0.

In the second modification named as Model 2, a moonpool is placed inside the body. The shape and dimension notations of the model are shown in the Figure 10.

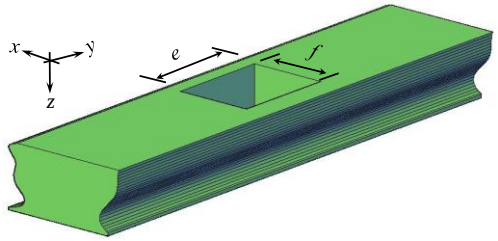

Figure 10 Model 2 shape

The value of *e* and *f* are same with the previous computation. This means that the volumes reduced in Model 1 and 2 are relatively similar. The computation results for Model 2 are shown in Figure 11.

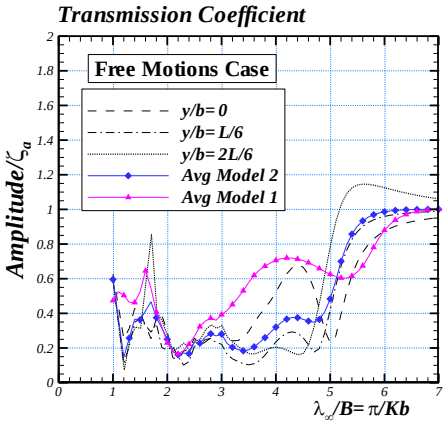

Figure 11 Transmission coefficients of Model 1 and 2

As can be seen from Figure 11, the model performance for this case is significantly improved as compared with the performance of Model 1. The performance improvement could be expected from motions and interaction of the incident wave inside the moonpoolwhich would reduce its energy thus reducing the transmitted waves.

However, several peaks in Figure 11 in shorter wavelength region can be noticed which are caused by the lack of number of panel used in computing this region.It is known that large numbers of panels are needed for computing high frequencies region. Another reason of the peaks could be what so-called irregular frequencies. In the previous study[10], an attempt to remove these frequencies are considered by placing some additional field points on the interior free surface of the body which is a method adopted by Haraguchi and Ohmatsu[15]. However, this technique seems not effective on removing these frequencies. Therefore, other methods should be implemented.

In order to obtain a more optimum performance model, the moonpool of the same volume is separated into two smaller moonpools. The shape and notations of the modified model for this case which is named as Model 3 are shown in Figure 12.

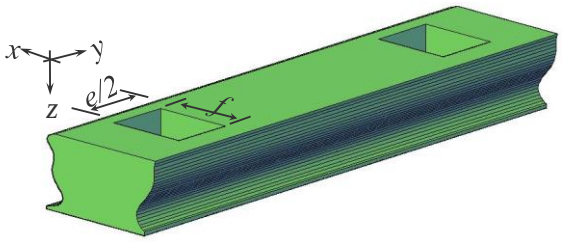

Figure 12 Model 3 shape

Computation results for Model 3 as compared to Model 2 computation results are shown in the following figure.

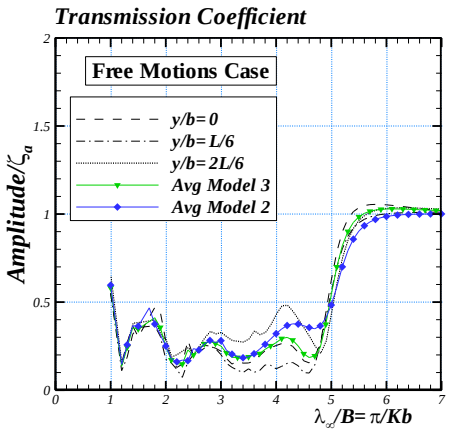

Figure 13 Transmission coefficients of Model 2 and 3

As shown in Figure 13, the performance of Model 3 is slightly better than performance of Model 2 especially in the wavelength range of λ_∞/B=3.8~4.6. However, it could also be noted that performance of Model 2 is slightly better than Model 3 in longer wavelength region. The smallchange of the performance is caused by the difference position of wave absorption due to change of the moonpools position. Consequently, in order to further optimize the model, it is important to evaluate the optimum size and locations of the moonpools. However, this topic is not discussed in the present study and will be left as a future work.

■5.0 CONCLUSION

Based on an original model which has an optimal performance, several models are constructed and computed in this study. Computation results show that a more realistic and efficient model for construction can be obtained by placing moonpools inside the body which allows reduction of model volume and material. Even though placing moonpools could negatively affect the model performance due to model shape change, motions and interaction of incident wave inside the moonpools could reduce the incident wave energy thus reducing the transmitted wave.

Acknowledgement

The author wouldlike to thank Professor Masashi Kashiwagi at Osaka University, Japan for fruitful discussion and valuable advice to author regarding the topicdiscussed in this paper whenthe author was conducting short term research program at Osaka University funded by JIBC/JICA.

References

[1] J. W. Van der Meer. 1993. *Conceptual Design of Rubble Mound Breakwaters*. Netherland: Delft Hydraulic.
[2] P. Bruun. 1985. *Design and Construction of Mounds for Breakwaters and Coastal Protection*. Netherland: Elsevier.
[3] W. F. Baird, K. R. Hall. 1984. *Canadian Journal of Civil Engineering*. 11: 164.
[4] Y. Goda, H. Takagi. 2000. *Coastal Engineering Journal*. 42: 357.
[5] H. Oumeraci, A. Kortenhaus. 1994. *Coastal Engineering*. 22: 159.
[6] K. Tanimoto, S. Takahashi. 1994. *Coastal Engineering*. 22: 57.
[7] L. Z. Hales. 1981. *Floating Breakwaters: State of the Art Literature Review*. Virginia: Coastal Engineering Research Center.
[8] B. McCartney. 1985. *J. Waterway, Port, Coastal, Ocean Eng.* 111: 304
[9] F. Mahmuddin, M. Kashiwagi. 2012. *Proc. of 22nd International Society of Offshore and Polar Engineers (ISOPE) Conference*. 33: 1263.
[10] M. Kashiwagi, F. Mahmuddin. 2012. *Proc. of 22nd International Society of Offshore and Polar Engineers (ISOPE) Conference*. 33: 1271.
[11] J. A. Helder, C. Schmittner, B. Buchner. 2012. *Proc. of Int. Conf. on Ocean, Offshore and Arctic Engineering*. 7: 547.
[12] G. Gaillarde, A. Cotteleer. 2004. *Water Motion in Moonpools Empirical and Theoretical Approach*. Association Technique Maritime etAeronautique (ATMA), Paris, France.
[13] M. Kashiwagi. 1995. *Bulletin Research Institute for Applied Mechanics, Kyushu University Japan*. 8: 98.
[14] M. Kashiwagi, *et al.* 2003. *3D Boundary Element Method; Chapter – 5 Practical Hydrodynamics of Floating Bodies*. SeizandoShoten, Co. Ltd. 129: 158
[15] T. Haraguchi, S. Ohmatsu. 1983. *Transaction of West-Japan Society of Naval Architecture*.